

SCIENTIFIC REPORTS



OPEN

Wave trains induced by circularly polarized electric fields in cardiac tissues

Xia Feng^{1,*}, Xiang Gao^{1,2,*}, Juan-Mei Tang¹, Jun-Ting Pan³ & Hong Zhang¹

Received: 12 February 2015

Accepted: 22 July 2015

Published: 25 August 2015

Clinically, cardiac fibrillation caused by spiral and turbulent waves can be terminated by globally resetting electric activity in cardiac tissues with a single high-voltage electric shock, but it is usually associated with severe side effects. Presently, a promising alternative uses wave emission from heterogeneities induced by a sequence of low-voltage uniform electric field pulses. Nevertheless, this method can only emit waves locally near obstacles in turbulent waves and thereby requires multiple obstacles to globally synchronize myocardium and thus to terminate fibrillation. Here we propose a new approach using wave emission from heterogeneities induced by a low-voltage circularly polarized electric field (i.e., a rotating uniform electric field). We find that, this approach can generate circular wave trains near obstacles and they propagate outwardly. We study the characteristics of such circular wave trains and further find that, the higher-frequency circular wave trains can effectively suppress spiral turbulence.

In hearts, spiral and turbulent waves may cause serious cardiac deceases, such as fibrillation^{1–7}. At present, the clinically effective method for terminating fibrillation uses a single high-voltage electric shock to reset all electric activity in cardiac tissues^{8–10}, but it is usually associated with severe side effects^{9–11}. Besides this method, a theoretical effort uses local fast pacing delivered via injecting a signal on a chosen area of the heart^{12–16}. Although this approach can numerically generate a higher-frequency wave train to suppress spiral turbulence, it is not easy to be realized in real cardiac tissues^{17–18}.

Recently, a promising alternative called wave emission from heterogeneities (WEH) or far-field stimulation is proposed^{19–21}. It exploits the fact that, applying an external electric field onto a whole piece of cardiac tissue can lead to de-polarizations and hyper-polarizations (so-called Weidmann zones²²) near obstacles. These obstacles can be considered as conductivity heterogeneities inherently in cardiac tissues such as blood vessels, ischemic regions, and smaller-scale discontinuities²³. If the de-polarizations are supra-threshold, these obstacles can act as virtual electrodes or second sources^{24–30}. Previous works focused on WEH in response to the uniform electric field (UEF)^{19–36}, which applies a sequence of low-voltage UEF pulses onto field electrodes. Nevertheless, WEH induced by UEF can only emit waves locally near obstacles in turbulent waves. So it requires multiple obstacles to activate more areas and progressively synchronize the whole myocardium to terminate fibrillation^{19–21}.

Compared to UEF, the circularly polarized electric field (CPEF) has shown its unique ability to control spirals and turbulence in chemical systems^{37–39}, which has been verified in the Belousov-Zhabotinsky reaction⁴⁰; with a different mechanism in cardiac tissues, CPEF can also unpin the anchored spirals⁴¹. In this paper, we study WEH in response to CPEF, and find it can generate circular wave trains (target waves) near obstacles and they can propagate outwardly. We study the capability of CPEF to induce such circular wave trains in a quiescent medium, and analyze the angular frequency relation between the circular wave

¹Zhejiang Institute of Modern Physics and Department of Physics, Zhejiang University, Hangzhou 310027, China.

²School of Physics and Information Technology, Shaanxi Normal University, Xi'an 710062, China. ³Institute of Physical Oceanography and Ocean College, Zhejiang University, Hangzhou 310058, China. *These authors contributed equally to this work. Correspondence and requests for materials should be addressed to H.Z. (email: hongzhang@zju.edu.cn)

trains and CPEF. Furthermore, we present a successful application of using a higher-frequency circular wave train induced by a low-voltage CPEF to suppress spiral turbulence, and also discuss its suppression mechanism.

Results

To describe the electric activity of cardiac tissues, we consider the following Luo-Rudy model⁴²:

$$\frac{\partial V}{\partial t} = -\frac{I_{ion}}{C_m} + \nabla \cdot (D\nabla V), \quad (1)$$

$$I_{ion} = I_{Na} + I_{si} + I_K + I_{K1} + I_{Kp} + I_b, \quad (2)$$

where V is the membrane potential, C_m is the membrane capacitance, D is the diffusion current coefficient, and I_{ion} is the total ionic currents which consist of a fast sodium current I_{Na} , a slow inward current I_{si} , a time-dependent potassium current I_K , a time-independent potassium current I_{K1} , a plateau potassium current I_{Kp} , and a time-independent background current I_b . In mono-domain models, the general effect of an external electric field on an obstacle can be expressed as a Neumann boundary condition^{36,43}: $\mathbf{n} \cdot (\nabla V - \mathbf{E}) = 0$, where \mathbf{n} is the normal vector to the obstacle boundary, and \mathbf{E} is the external electric field. Through this paper without loss of generality, we choose $\mathbf{E} = (E_x, E_y)$ as a counter-clockwise rotating CPEF, where $E_x = E_0 \cos(\omega_{CPEF}t)$, $E_y = E_0 \cos(\omega_{CPEF}t + 3\pi/2)$, and E_0 , ω_{CPEF} are its strength and angular frequency, respectively.

In the following, we use a two-dimensional quiescent medium with a circular obstacle of radius R in its center to do the simulation. We find that, as shown in Fig. 1a,b, with CPEF at a weak strength E_0 and certain frequency ω_{CPEF} , the de-polarization and hyper-polarization induced by CPEF near the obstacle rotate synchronously with the rotating CPEF, and the membrane potential pattern is distributed similarly as Chinese “ancient Taijitu”⁴¹. When E_0 increases above some threshold, the de-polarization begins to emit a wave as shown in Fig. 1c,d. Then the two ends of the wave propagate oppositely along the obstacle, and they quickly collide with each other and finally can form a circular wave propagating outwardly as shown in Fig. 1e. With the continued effect of CPEF, the second circular wave can be formed and it can also propagate outwardly, then the third one and so on can also emerge (see Fig. 1f). That is, a circular wave train can be generated and can continually propagate outwardly. Similarly, we also observe a circular wave train induced by CPEF near a circular obstacle in a modified FitzHugh-Nagumo model⁴⁴, thus the above results may be model-independent. Therefore, we can recognize that an obstacle under CPEF can act as a pacing electrode and generate the circular wave train.

As for such a circular wave train induced by CPEF, for convenience, we focus on studying the formation time (T) of the first circular wave to reflect the capability of CPEF to induce the circular wave train. As illustrated in Fig. 2, with a given angular frequency of CPEF, we can find T is highly related to R and E_0 . In details, with a given E_0 , the reciprocal of $T(1/T)$ will change when R increases. As shown in Fig. 2a, with $E_0 = 1.0$ V/cm, we can see R has a threshold at 0.04 cm, and $1/T$ has a sharp up jump. Below this threshold, $1/T$ is zero, which means no wave can be induced by CPEF near such small obstacles. Once R increases above this threshold, $1/T$ begins to decrease. And with the continual increasing of R , $1/T$ decreases more and more slowly. On the other hand, with a given R , $1/T$ will also change when E_0 increases. As shown in Fig. 2b, with $R = 0.24$ cm, E_0 also has a threshold at 0.45 V/cm, and $1/T$ also has a sharp up jump. Below this threshold, $1/T$ is zero and no wave can be induced by CPEF because the electric strength is not strong enough to exceed the de-polarization threshold. Once E_0 increases above this threshold, $1/T$ begins to increase slowly. And if E_0 becomes large enough (e.g. $E_0 = 0.85$ V/cm as illustrated in Fig. 2b), $1/T$ tends to be a constant.

With proper R and E_0 , the circular waves can be continuously induced by CPEF and then can form a circular wave train with angular frequency ω_{cir} . Since the circular wave train is forcedly excited by CPEF with ω_{CPEF} , ω_{cir} should highly depend on ω_{CPEF} . In Fig. 3a, to study the relation between ω_{cir} and ω_{CPEF} , we gradually increase ω_{CPEF} from 0.065 rad/ms which can be seen as a minimum (Below this minimum, CPEF cannot generate a stable circular wave train). When ω_{CPEF} is set as this minimum, a stable circular wave train can be generated and its angular frequency ω_{cir} is synchronized with ω_{CPEF} , and the ratio $\omega_{CPEF}/\omega_{cir}$ is about 1:1 as shown in Fig. 3b. However, when ω_{CPEF} increases above 0.07 rad/ms, ω_{cir} has a down jump (see Fig. 3a) which leads the ratios $\omega_{CPEF}/\omega_{cir}$ are no longer 1:1 but locked at nearly 2:1 (see Fig. 3b). The reason for this is that, CPEF rotates so fast that after forming a circular wave, the medium around the obstacle has not yet recovered to be excitable. Thus the rotating de-polarization of CPEF cannot excite another wave in its present round until the medium recover to be excitable again in its next round, and so forth. If ω_{CPEF} continues to increase, ω_{cir} will also increase but the ratios $\omega_{CPEF}/\omega_{cir}$ are always locked at nearly 2:1 until ω_{CPEF} reaches 0.17 rad/ms. When ω_{CPEF} becomes larger than 0.17 rad/ms, ω_{cir} faces another down jump and subsequently another increasing with ω_{CPEF} , and the ratios $\omega_{CPEF}/\omega_{cir}$ are locked at nearly 3:1. In a word, as illustrated in Fig. 3, CPEF always keeps nearly $n:1$ ($n = 1, 2, 3$) angular frequency relation with the induced circular wave train, which has been widely reported in the pattern formation domain^{45–48}.

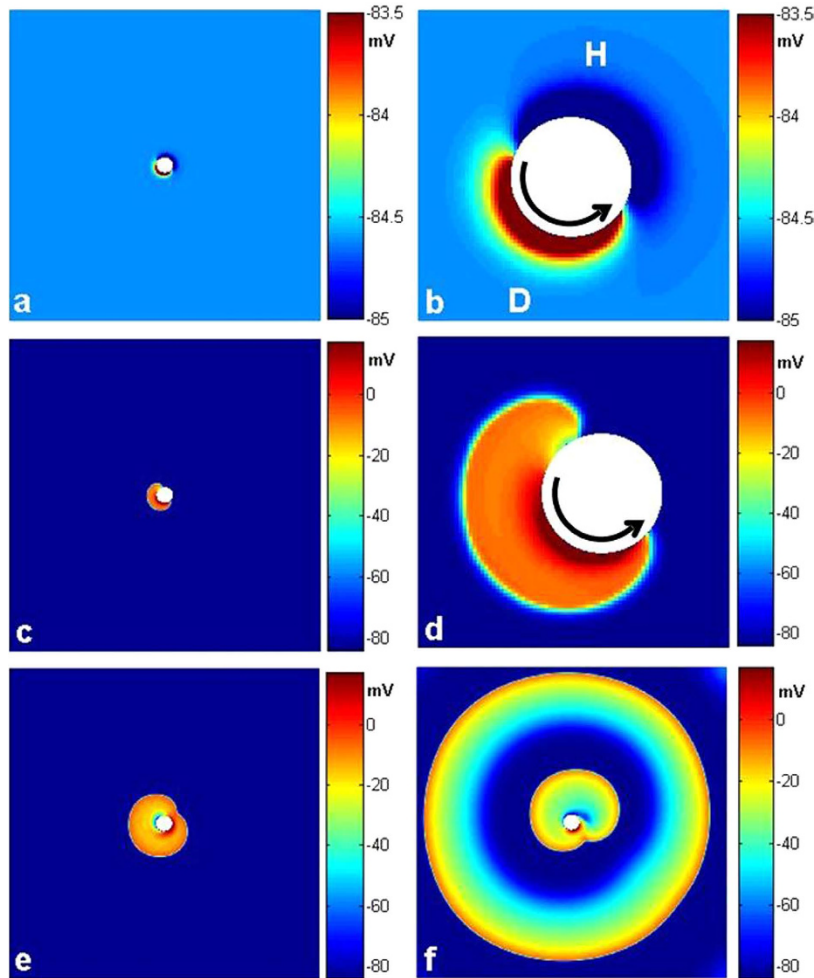


Figure 1. Circular waves induced by CPEF in a two-dimensional quiescent medium. The angular frequency of CPEF $\omega_{CPEF} = 0.14$ rad/ms and the obstacle radius $R = 0.24$ cm. (a,b), Distribution of the membrane potential induced by CPEF with strength $E_0 = 0.1$ V/cm. (c,d), A wave induced by de-polarization under CPEF with $E_0 = 1.0$ V/cm. (e), The first circular wave induced by CPEF. (f), The second and the third circular waves induced by CPEF. The patterns in (b,d) are the enlarged views of those in (a,c), respectively. Regions D and H represent de-polarization and hyper-polarization induced by CPEF, respectively. The black curved arrows mean that CPEF rotate counter-clockwise.

Besides, we also measure the dominant angular frequency of the spiral turbulence ω_{tur} in the same medium and the same obstacle. We can see from Fig. 3a that, in some angular frequency ranges of ω_{CPEF} , ω_{cir} is higher than ω_{tur} . As the high-frequency waves may invade low-frequency domain^{49–56}, we believe the circular wave trains with such higher frequencies can suppress spiral turbulence^{12–18}.

To test this idea we choose $E_0 = 1.0$ V/cm, $\omega_{CPEF} = 0.14$ rad/ms for CPEF which can generate the circular wave train with angular frequency ω_{cir} higher than ω_{tur} (see Fig. 3a). In Fig. 4, we numerically simulate spiral turbulence with a circular obstacle of $R = 0.24$ cm and use it as the initial state ($t = 0$). In the beginning of applying CPEF, due to the disturbance of the nearby turbulent waves, the emitted waves near the obstacle fail to form circular waves. Nevertheless, by continuously emitting waves under CPEF, circular waves begin to emerge. Then at $t = 1000$ ms, a full circular wave is formed and squeezes out the nearby turbulent waves, following which more and more circular waves can be gradually formed. Later at $t = 1800$ ms, there are only few turbulent waves left. Finally at $t = 2800$ ms, all the turbulent waves are driven away out of the boundary. In addition, the medium can recover to a quiescent state after stopping CPEF. Furthermore, we find the circular wave trains induced by CPEF can successfully suppress spiral turbulence as long as $\omega_{cir} > \omega_{tur}$. Similarly in the modified FitzHugh-Nagumo model, the higher-frequency circular wave train induced by CPEF near a circular obstacle is also obtained and it can also successfully suppress the spiral turbulence.

Furthermore, we also testify the ability of CPEF suppressing three-dimensional scroll turbulence in Luo-Rudy model. As illustrated in Fig. 5, we numerically simulate scroll turbulence with a spherical obstacle of $R = 0.24$ cm as the initial state ($t = 0$). Then under CPEF, emitting waves continuously emerge

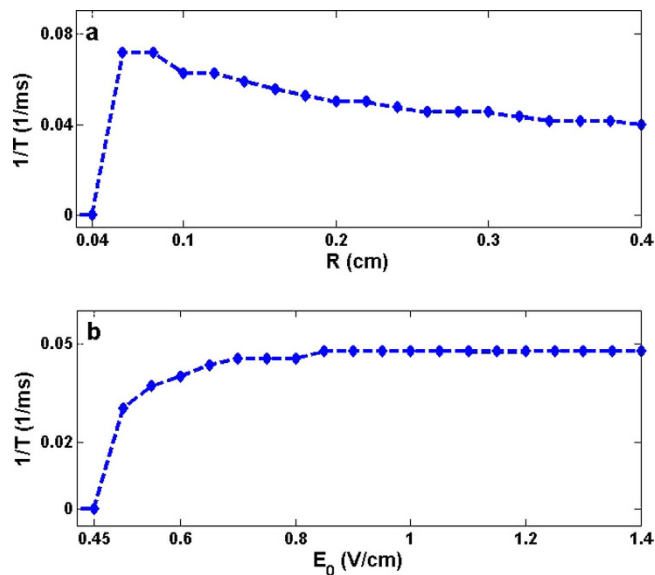


Figure 2. The formation time (T) of the first circular wave induced by CPEF in a two-dimensional quiescent medium. (a), The relation between $1/T$ and the obstacle radius R , where the strength of CPEF $E_0 = 1.0 \text{ V/cm}$. (b), The relation between $1/T$ and E_0 , where $R = 0.24 \text{ cm}$. The angular frequency of CPEF $\omega_{\text{CPEF}} = 0.14 \text{ rad/ms}$ in both (a,b).

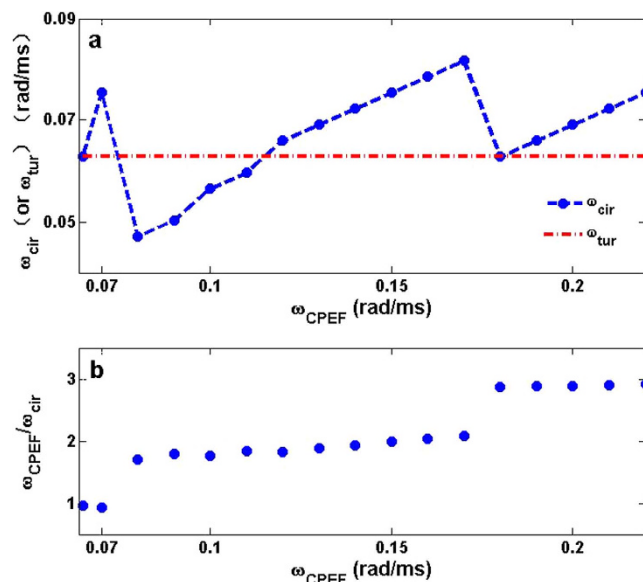


Figure 3. The angular frequency relations between the circular wave train and CPEF in a two-dimensional quiescent medium. (a), The obstacle radius $R = 0.24 \text{ cm}$, the strength of CPEF $E_0 = 1.0 \text{ V/cm}$, and the angular frequency of CPEF $0.065 \text{ rad/ms} \leq \omega_{\text{CPEF}} \leq 0.22 \text{ rad/ms}$. The dashed line with solid circles represents the angular frequency of the circular wave trains ω_{cir} . The dash-dotted line represents the dominant angular frequency of the spiral turbulence ω_{tur} in the same medium and the same obstacle. (b), The ratios of ω_{CPEF} over ω_{cir} correspond to the data in (a).

and collide with the turbulent waves ($t = 650 \text{ ms}$). Later at $t = 890 \text{ ms}$, a full spherical wave is formed and squeezes out the nearby turbulent waves. Finally at $t = 1100 \text{ ms}$, all the turbulent waves are driven away out of the boundary. Similarly, we also observe that, in the modified FitzHugh-Nagumo model, a spherical wave train induced by CPEF near a spherical obstacle can successfully suppress the three-dimensional scroll turbulence.

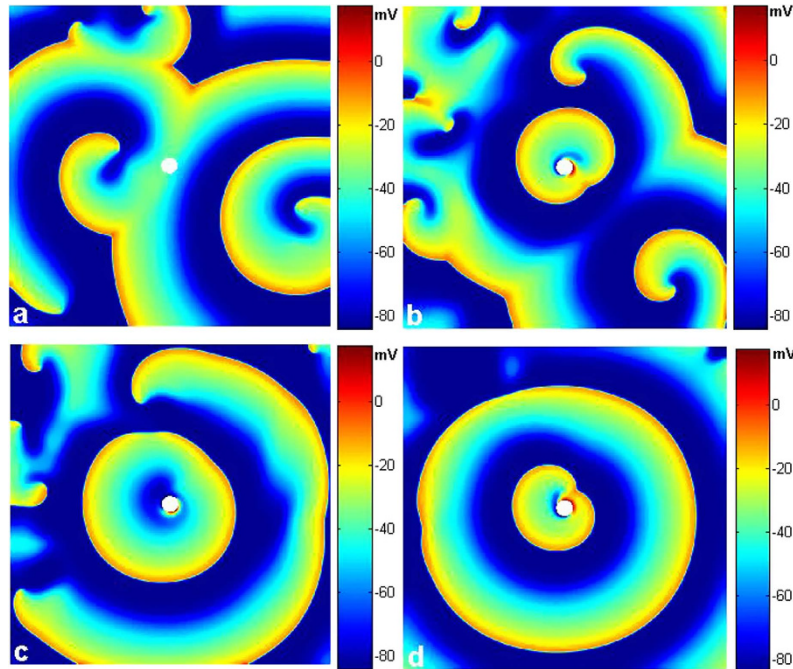


Figure 4. Suppression of two-dimensional spiral turbulence by CPEF. The obstacle radius $R=0.24$ cm, and the dominant angular frequency of the spiral turbulence ω_{tur} is the same as that in Fig. 3a. The strength of CPEF $E_0=1.0$ V/cm and the angular frequency of CPEF $\omega_{CPEF}=0.14$ rad/ms. (a), The CPEF is applied from $t=0$. (b), $t=1000$ ms. (c), $t=1800$ ms. (d), $t=2800$ ms.

Discussion

In this section, we discuss the mechanism about successfully suppressing the spiral turbulence by a high-frequency circular wave train induced by CPEF. And we can owe this success to the contributions of the rotating de-polarization and hyper-polarization induced by CPEF, thus the membrane potential at the boundary of the obstacle would successively and periodically go through both effects. Under the influence of CPEF ($E_0=1.0$ V/cm, $\omega_{CPEF}=0.14$ rad/ms, the same as those in Fig. 4), we study the variation of the membrane potential at an arbitrary position on the obstacle boundary in a quiescent medium, e.g., the membrane potential V1 in Fig. 6a. We find V1 would be depolarized to the excited state, and then forced to recover to the excitable state quickly by the hyper-polarization as shown in Fig. 6b. Due to the diffusion of V1, the nearby membrane potential V2 would also be directly affected. Although the second stimulus from V1 fails to de-polarize V2, the effect of hyper-polarization from V1 still makes it recovered to the excitable state quickly. Thus V2 is able to be de-polarized by the third stimulus from V1. Further, the membrane potential V3 would be affected by the diffusion of V2 and thus forms periodic excitations (i.e., the circular wave train). Hence every two rounds of the rotating de-polarization and hyper-polarization induced by CPEF can stimulate a circular wave. The angular frequency of the circular wave train ω_{cir} is 0.072 rad/ms, which is higher than ω_{tur} . Therefore, the circular wave train induced by CPEF with such a high angular frequency can be used to suppress the spiral turbulence.

As shown in Fig. 1A of Ref. 35, using UEF can also generate circular waves near the obstacle in a quiescent medium. However, UEF can hardly utilize the same mechanism as CPEF to induce a higher-frequency circular wave train for suppressing the spiral turbulence. We employ a series of UEF pulses to the quiescent medium with the same electric strength and angular frequency as CPEF. In Fig. 6c, we find the membrane potential V1 excited by the de-polarization induced by UEF cannot be forced to recover to the excitable state quickly due to the lack of the hyper-polarization in the same position, thus the nearby membrane potential V2 will have to go through a relatively long excited time. Hence the membrane potential V2 and thereby V3 can only be stimulated for every three UEF pulses. As illustrated in Fig. 6d, the membrane potential V4 is only affected by the hyper-polarization induced by UEF which cannot induce stimuli and the existing stimuli actually come from V1. So the ratio $\omega_{UEF}/\omega_{cir}$ is about 3:1 and ω_{cir} is about 0.047 rad/ms, which is lower than ω_{tur} . Therefore UEF at $\omega_{UEF}=0.14$ rad/ms cannot induce a higher-frequency circular wave train to suppress the spiral turbulence.

In order to verify whether UEF with other ω_{UEF} can induce higher-frequency circular wave trains, we measure ω_{cir} in a large region of ω_{UEF} in the same quiescent medium and the same obstacle as in Fig. 3a. As shown in Fig. 7a, most of the circular wave trains induced by UEF have $\omega_{cir}<\omega_{tur}$ and thus cannot suppress the spiral turbulence. Comparing it to the case of CPEF in Fig. 3a and taking the angular frequency ranges of 0.13 rad/ms $\leq \omega \leq 0.17$ rad/ms for instance, we find every two rounds of CPEF can

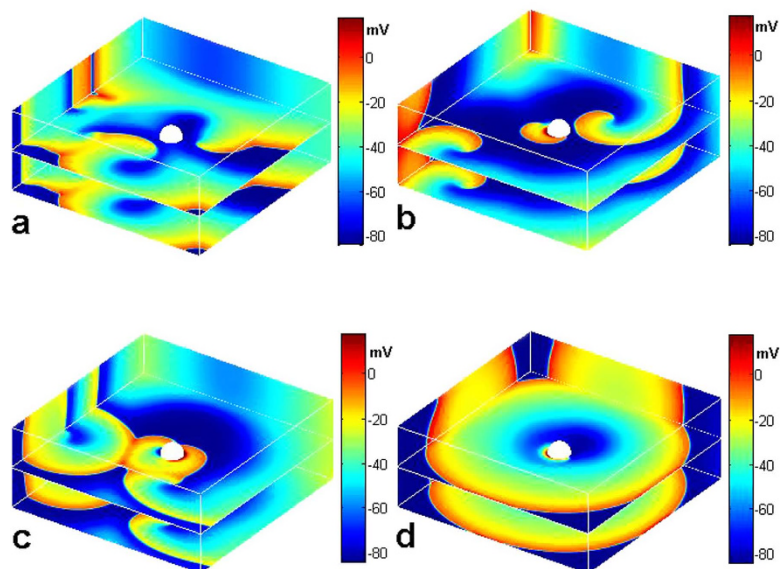


Figure 5. Suppression of three-dimensional scroll turbulence by CPEF. The obstacle radius $R=0.24$ cm. The strength of CPEF $E_0=1.8$ V/cm and the angular frequency of CPEF $\omega_{CPEF}=0.14$ rad/ms. (a), The CPEF is applied from $t=0$. (b), $t=650$ ms. (c), $t=890$ ms. (d), $t=1100$ ms.

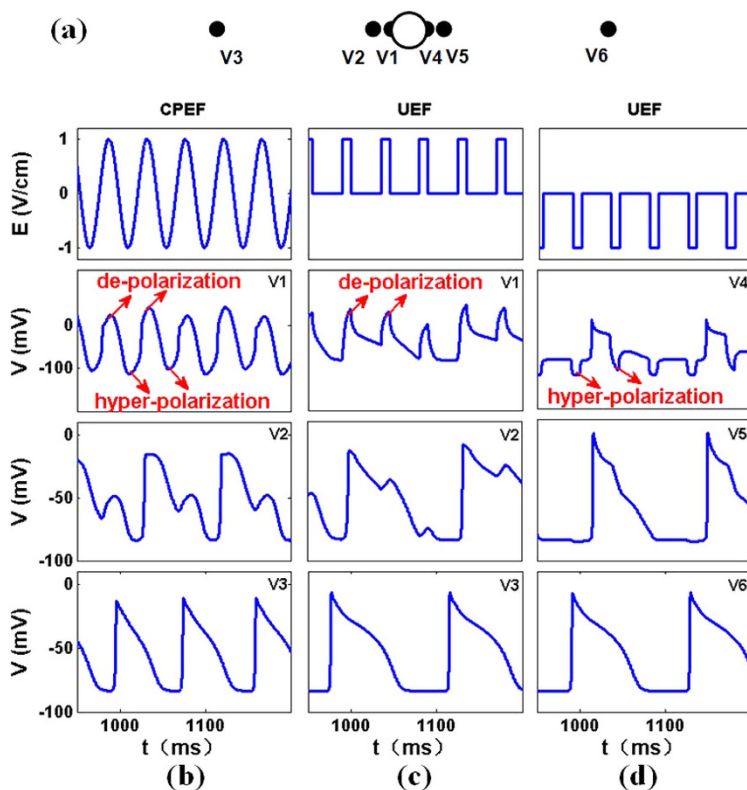


Figure 6. The variations of the membrane potentials V under CPEF or UEF in a two-dimension quiescent medium. (a), The locations of the membrane potentials V1-V6. V1, V4 are the membrane potentials on the obstacle boundary. V2, V5 are the membrane potentials near the obstacle boundary. V3, V6 are the membrane potentials far away from the obstacle boundary. CPEF rotates counter-clockwise and UEF is horizontal. (b), Under CPEF, the strength $E_0=1.0$ V/cm and the angular frequency $\omega_{CPEF}=0.14$ rad/ms. (c,d), Under UEF, $E_0=1.0$ V/cm, $\omega_{UEF}=0.14$ rad/ms, and the pulse duration is 10 ms. The red arrows indicate the effects of the de-polarizations and hyper-polarizations.

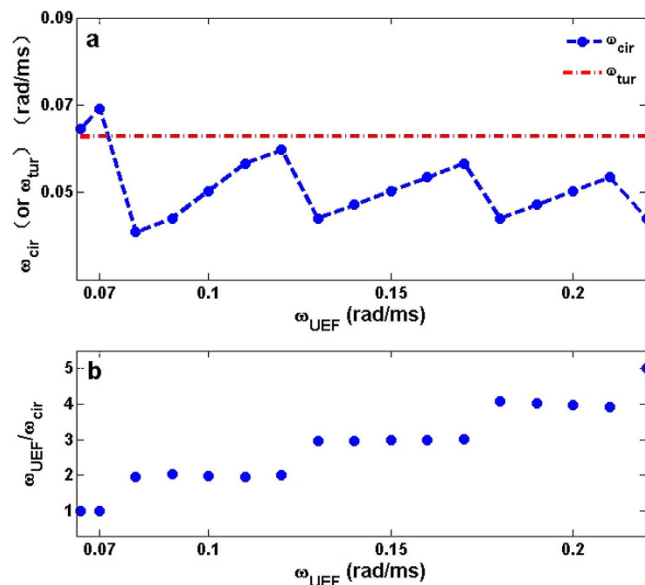


Figure 7. The angular frequency relations between the circular wave trains and UEF in a two-dimension quiescent medium. (a), The obstacle radius $R = 0.24$ cm, the strength of UEF $E_0 = 1.0$ V/cm, the angular frequency of UEF $0.065 \text{ rad/ms} \leq \omega_{UEF} \leq 0.22 \text{ rad/ms}$, and the pulse duration is 10 ms. The dashed line with solid circles represents the angular frequency of the circular wave trains ω_{cir} . The dash-dotted line represents the dominant angular frequency of the spiral turbulence ω_{tur} in the same medium and the same obstacle. (b), The ratios of ω_{UEF} over ω_{cir} correspond to the data in (a).

stimulate a circular wave, but UEF at the same angular frequency would need three pulses to stimulate a circular wave (may refer to Figs 3b and 7b), and thus $\omega_{cir}(UEF) < \omega_{tur} < \omega_{cir}(CPEF)$.

In other words, the main difference of CPEF from UEF is the rotation. Because of the rotation of CPEF, the medium will be affected by both de-polarization and hyper-polarization. While using UEF, only the de-polarization can affect the medium. Therefore, with the same angular frequency of both external electric fields ($\omega = 0.14 \text{ rad/ms}$ in Fig. 6), the ratio $\omega_{CPEF}/\omega_{cir}$ is about 2:1, as shown in Fig. 6b. However, the ratio $\omega_{UEF}/\omega_{cir}$ is about 3:1, as illustrated in Fig. 6c. Hence the circular wave train induced by the rotating CPEF has the angular frequency of $\omega_{cir}(CPEF) = 0.072 \text{ rad/ms}$ which is higher than $\omega_{cir}(UEF) = 0.047 \text{ rad/ms}$. And this difference of ratios between CPEF and UEF exists in a wide region of the angular frequency ω of both external electric fields. Comparing with the Figs 3a and 7a, the rotating CPEF can maintain the phase-locking state at the ratio of 2:1 in a longer region than UEF. And in some part of the ratio of 2:1 (i.e., $0.13 \text{ rad/ms} \leq \omega \leq 0.17 \text{ rad/ms}$), the circular wave trains induced by CPEF have higher frequencies than the dominant frequency of turbulence and can be used to terminate fibrillation. But in the same region (i.e., $0.13 \text{ rad/ms} \leq \omega \leq 0.17 \text{ rad/ms}$), the circular wave trains induced by UEF are at the ratio of 3:1, and thus have lower frequencies than the dominant frequency of turbulence, and cannot be used to terminate fibrillation.

Moreover, further simulations indicate the waves induced by UEF cannot form the circular waves in the turbulent waves and thereby the induced circular wave trains in the quiescent medium with relatively high angular frequencies ($\omega_{cir} = 0.07 \text{ rad/ms}$ in Fig. 7) also cannot suppress the spiral turbulence as in Fig. 4. This may owe to the fact that the de-polarization and hyper-polarization induced by UEF cannot rotate and thus the waves can only be induced in a fixed position near the obstacle (e.g., only V1 in Fig. 6c affected by the de-polarization can emit waves while V4 in Fig. 6d cannot). Conversely, the de-polarization and hyper-polarization induced by CPEF can rotate and thereby the waves can be emitted in any position on the obstacle boundary (e.g., the membrane potential at the arbitrary position on the obstacle boundary has the same variation as V1 in Fig. 6b). Hence CPEF can effectively generate the circular wave trains and eventually suppress the turbulent waves. Therefore, although the circular wave trains can be induced by UEF in a quiescent medium, they cannot form the circular waves in the presence of turbulence waves as in Fig. 4 and thereby UEF can hardly utilize the same mechanism as CPEF to suppress spiral turbulence.

To conclude, CPEF can effectively generate the higher-frequency circular wave trains near obstacles. And this capability is closely related to the strength and the angular frequency of CPEF and the size of obstacles. Moreover, the circular wave trains induced by CPEF have a wide application prospect. An important application is that the higher-frequency circular wave trains induced by CPEF can be used to suppress spiral turbulence, which may provide a promising alternative to terminate fibrillation. Additionally, CPEF has been realized in Belousov-Zhabotinsky reaction by applying two ACs onto two pairs of field electrodes perpendicular to each other⁴⁰. Similarly, it will also be easily realized in cardiac

tissues by replacing DCs to ACs in the experimental preparation of Fig. 5D in Ref. 20. Hence we believe this approach will have strong practical value in heart clinical treatments, and its effectiveness and applicability in bi-domain model and in real cardiac tissues will need to be further studied.

Methods

In Luo-Rudy model, to add the introduced boundary condition into the circular boundary of the obstacle in Cartesian coordinates, we adopt the phase field method^{36,43}. Considering the effect of an external electric field on the obstacle, equation (1) can be adapted as

$$\frac{\partial V}{\partial t} = -\frac{I_{ion}}{C_m} + D\nabla \cdot (\nabla V) + D(\nabla(\ln \phi) \cdot (\nabla V)) - D(\nabla(\ln \phi) \cdot \mathbf{E}) \quad (3)$$

where $C_m = 1 \mu\text{F}/\text{cm}^2$, $D = 0.001 \text{ cm}^2/\text{ms}$, the total ionic currents I_{ion} are determined by ionic gates, whose gating variables are obtained as solutions to a coupled system of nonlinear ordinary differential equations, and the parameters are modified as in Ref. 57. In Cartesian coordinates, equation (3) is integrated on the $10 \text{ cm} \times 10 \text{ cm}$ two-dimensional medium and $5 \text{ cm} \times 5 \text{ cm} \times 2 \text{ cm}$ three-dimensional medium which are large enough to sustain the turbulence^{57–59} with no-flux boundary conditions via Euler method, and the central difference method is applied to compute the Laplacian term $\nabla^2 V$ and the gradient terms $\nabla(\ln \phi)$, ∇V . The space and the time step in two-dimensional domain are $\Delta x = 0.015 \text{ cm}$, $\Delta y = 0.015 \text{ cm}$ and $\Delta t = 0.005 \text{ ms}$, respectively. And the space and the time step in three-dimensional domain are $\Delta x = 0.02 \text{ cm}$, $\Delta y = 0.02 \text{ cm}$, $\Delta z = 0.02 \text{ cm}$ and $\Delta t = 0.01 \text{ ms}$, respectively.

References

1. Winfree, A. T. *When Time Breaks Down*. (Princeton NJ: Princeton University Press, 1987).
2. Davidenko, J. M., Pertsov, A. V., Salomonsz, R., Baxter, W. & Jalife, J. Stationary and drifting spiral waves of excitation in isolated cardiac-muscle. *Nature* **355**, 349–351 (1992).
3. Gray, R. A., Pertsov, A. M. & Jalife, J. Spatial and temporal organization during cardiac fibrillation. *Nature* **392**, 75–78 (1998).
4. Witkowski, F. X. *et al.* Spatiotemporal evolution of ventricular fibrillation. *Nature* **392**, 78–82 (1998).
5. Jalife, J. Ventricular fibrillation: mechanisms of initiation and maintenance. *Annu. Rev. Physiol.* **62**, 25–50 (2000).
6. Cherry, E. M. & Fenton, F. H. Visualization of spiral and scroll waves in simulated and experimental cardiac tissue. *New J. Phys.* **10**, 125016 (2008).
7. Karma, A. Physics of cardiac arrhythmogenesis. *Annu. Rev. Condens. Matter Phys.* **4**, 313–337 (2013).
8. Koster, R. W. *et al.* A randomized trial comparing monophasic and biphasic waveform shocks for external cardioversion of atrial fibrillation. *Am. Heart J.* **147**, e1–e7 (2004).
9. Babbs, C. F., Tacker, W. A., VanVleet, J. F., Bourland, J. D. & Geddes, L. A. Therapeutic indices for transthoracic defibrillator shocks: effective, damaging, and lethal electrical doses. *Am. Heart J.* **99**, 734–738 (1980).
10. Santini, M. *et al.* Single shock endocavitary lowenergy intracardiac cardioversion of chronic atrial fibrillation. *J. Interv. Card. Electrophysiol.* **3**, 45–51 (1999).
11. Walcott, G. P., Killingsworth, C. R. & Ideker, R. E. Do clinically relevant transthoracic defibrillation energies cause myocardial damage and dysfunction? *Resuscitation* **59**, 59–70 (2003).
12. Zhang, H., Hu, B. B. & Hu, G. Suppression of spiral waves and spatiotemporal chaos by generating target waves in excitable media. *Phys. Rev. E* **68**, 026134 (2003).
13. Zhang, H., Cao, Z. J., Wu, N. J., Ying, H. P. & Hu, G. Suppress Winfree turbulence by local forcing excitable systems. *Phys. Rev. Lett.* **94**, 188301 (2005).
14. Yuan, G. Y., Wang, G. R. & Chen, S. G. Control of spiral waves and spatiotemporal chaos by periodic perturbation near the boundary. *Europhys. Lett.* **72**, 908–914 (2005).
15. Cao, Z. J., Li, P. F., Zhang, H., Xie, F. G. & Hu, G. Turbulence control with local pacing and its implication in cardiac defibrillation. *Chaos* **17**, 015107 (2007).
16. Tang, G. N., Deng, M. Y., Hu, B. B. & Hu, G. Active and passive control of spiral turbulence in excitable media. *Phys. Rev. E* **77**, 046217 (2008).
17. Wathen, M. S. *et al.* Prospective randomized multicenter trial of empirical antitachycardia pacing versus shocks for spontaneous rapid ventricular tachycardia in patients with implantable cardioverter-defibrillators—Pacing Fast Ventricular Tachycardia Reduces Shock Therapies (PainFREE Rx II) trial results. *Circulation* **110**, 2591–2596 (2004).
18. Qu, Z. L., Hu, G., Garfinkel, A. & Weiss, J. N. Nonlinear and stochastic dynamics in the heart. *Phys. Rep.* **543**, 61–162 (2014).
19. Pumir, A. *et al.* Wave emission from heterogeneities opens a way to controlling chaos in the heart. *Phys. Rev. Lett.* **99**, 208101 (2007).
20. Fenton, F. H. *et al.* Termination of atrial fibrillation using pulsed low-energy far-field stimulation. *Circulation* **120**, 467–476 (2009).
21. Luther, S. *et al.* Low-energy control of electrical turbulence in the heart. *Nature* **475**, 235–239 (2011).
22. Weidmann, S. Effect of current flow on the membrane potential of cardiac muscle. *J. Physiol.* **115**, 227–236 (1951).
23. Plonsey, R. The nature of sources of bioelectric and biomagnetic fields. *Biophys. J.* **39**, 309–312 (1982).
24. Sepulveda, N. G., Roth, B. J. & Wikswo, J. P. Current injection into a two-dimensional anisotropic bidomain. *Biophys. J.* **55**, 987–999 (1989).
25. Sobie, E. A., Susil, R. C. & Tung, L. A generalized activating function for predicting virtual electrodes in cardiac tissue. *Biophys. J.* **73**, 1410–1423 (1997).
26. Fishler, M. G. Syncytial heterogeneity as a mechanism underlying cardiac far-field stimulation during defibrillation-level shocks. *J. Cardiovasc. Electr.* **9**, 384–394 (1998).
27. Fast, V. G., Rohr, S., Gillis, A. M. & Kléber, A. G. Activation of cardiac tissue by extracellular electrical shocks: Formation of ‘secondary sources’ at intercellular clefts in monolayers of cultured myocytes. *Circ. Res.* **82**, 375–385 (1998).
28. Trayanova, N. & Skouibine, K. Modeling defibrillation—Effects of fiber curvature. *J. Electrocardiol.* **31**, 23–29 (1998).
29. Hooks, D. A. *et al.* Cardiac microstructure: Implications for electrical propagation and defibrillation in the heart. *Circ. Res.* **91**, 331–338 (2002).

30. Woods, M. C. *et al.* Virtual electrode effects around an artificial heterogeneity during field stimulation of cardiac tissue. *Heart Rhythm* **3**, 751–752 (2006).
31. Pumir, A. & Krinsky, V. Unpinning of a rotating wave in cardiac muscle by an electric field. *J. Theor. Biol.* **199**, 311–319 (1999).
32. Takagi, S. *et al.* Unpinning and removal of a rotating wave in cardiac muscle. *Phys. Rev. Lett.* **93**, 058101 (2004).
33. Ripplinger, C. M., Krinsky, V. I., Nikolski, V. P. & Efimov, I. R. Mechanisms of unpinning and termination of ventricular tachycardia. *Am. J. Physiol. Heart Circ. Physiol.* **291**, H184–H192 (2006).
34. Bittihn, P. *et al.* Far field pacing supersedes anti-tachycardia pacing in a generic model of excitable media. *New J. Phys.* **10**, 103012 (2008).
35. Cysyk, J. & Tung, L. Electric field perturbations of spiral waves attached to millimeter-size obstacles. *Biophys. J.* **94**, 1533–1541 (2008).
36. Bittihn, P., Hörning, M. & Luther, S. Negative curvature boundaries as wave emitting sites for the control of biological excitable media. *Phys. Rev. Lett.* **109**, 118106 (2012).
37. Cai, M. C., Pan, J. T. & Zhang, H. Electric-field-sustained spiral waves in subexcitable media. *Phys. Rev. E* **86**, 016208 (2012).
38. Li, B. W., Deng, L. Y. & Zhang, H. Chiral symmetry breaking in a reaction-diffusion system. *Phys. Rev. E* **87**, 042905 (2013).
39. Li, B. W., Cai, M. C., Zhang, H., Panfilov, A. V. & Dierckx, H. Chiral selection and frequency response of spiral waves in reaction-diffusion systems under a chiral electric field. *J. Chem. Phys.* **140**, 184901 (2014).
40. Ji, L., Zhou, Y., Li, Q., Qiao, C. & Ouyang, Q. Experimental evidence of using a circularly polarized electric field to control spiral turbulence. *Phys. Rev. E* **88**, 042919 (2013).
41. Feng, X., Gao, X., Pan, D. B., Li, B. W. & Zhang, H. Unpinning of rotating spiral waves in cardiac tissues by circularly polarized electric fields. *Sci. Rep.* **4**, 04831 (2014).
42. Luo, C. H. & Rudy, Y. A model of the ventricular cardiac action potential depolarization, repolarization, and their interaction. *Circ. Res.* **68**, 1501–1526 (1991).
43. Bittihn, P. Complex structure and dynamics of the heart, PhD thesis, Georg-August-Universität Göttingen (2013).
44. Bär, M. & Eiswirth, M. Turbulence due to spiral breakup in a continuous excitable medium. *Phys. Rev. E* **48**, R1635–R1637 (1993).
45. Petrov, V., Ouyang, Q. & Swinney, H. L. Resonant pattern formation in a chemical system. *Nature* **388**, 655 (1997).
46. Lin, A. L., Bertram, M., Martinez, K. & Swinney, H. L. Resonant phase patterns in a reaction-diffusion system. *Phys. Rev. Lett.* **84**, 4240 (2000).
47. Steinbock, O., Zykov, V. & Müller, S. C. Control of spiral-wave dynamics in active media by periodic modulation of excitability. *Nature* **366**, 322 (1993).
48. Braune, M., Schrader, A. & Engel, H. Entrainment and resonance of spiral waves in active media with periodically modulated excitability. *Chem. Phys. Lett.* **222**, 358 (1994).
49. Hendrey, M., Ott, E. & Antonsen, T. M. Jr. Effect of inhomogeneity on spiral wave dynamics. *Phys. Rev. Lett.* **82**, 859 (1999).
50. Hendrey, M., Ott, E. & Antonsen, T. M. Jr. Spiral wave dynamics in oscillatory inhomogeneous media. *Phys. Rev. E* **61**, 4943 (2000).
51. Lee, K. J. Wave pattern selection in an excitable system. *Phys. Rev. Lett.* **79**, 2907 (1997).
52. Xie, F. G., Qu, Z. L., Weiss, J. N. & Garfinkel, A. Interactions between stable spiral waves with different frequencies in cardiac tissue. *Phys. Rev. E* **59**, 2203 (1999).
53. Zhang, C. X., Liao, H. M., Zhou, L. Q. & Ouyang, Q. Pattern selection in the Belousov-Zhabotinsky reaction with the addition of an activating reactant. *J. Phys. Chem. B* **108**, 16990 (2004).
54. Smolka, L. B., Marts, B. & Lin, A. L. Effect of inhomogeneities on spiral wave dynamics in the Belousov-Zhabotinsky reaction. *Phys. Rev. E* **72**, 056205 (2005).
55. Kheowan, O.-U., Mihaliuk, E., Blasius, B., Sendiña-Nadal, I. & Showalter, K. Wave mediated synchronization of nonuniform oscillatory media. *Phys. Rev. Lett.* **98**, 074101 (2007).
56. Luo, J. M., Zhang, B. S. & Zhan, M. Frozen state of spiral waves in excitable media. *Chaos* **19**, 033133 (2009).
57. Qu, Z. L., Xie, F. G., Garfinkel, A. & Weiss, J. N. Origins of spiral wave meander and breakup in a two-dimensional cardiac tissue model. *Ann. Biomed. Eng.* **28**, 755–771 (2000).
58. Qu, Z. L., Kil, J., Xie, F. G., Garfinkel, A. & Weiss, J. N. Scroll wave dynamics in a three-dimensional cardiac tissue model: roles of restitution, thickness, and fiber rotation. *Biophys. J.* **78**, 2761–2775 (2000).
59. Alonso, S. & Panfilov, A. V. Negative filament tension in the Luo-Rudy model of cardiac tissue. *Chaos* **17**, 015102 (2007).

Acknowledgements

We would like to thank Alain Pumir for his helpful discussions. This work was supported by the National Natural Science Foundation of China under Grants No. 11275167, No. 11447026 and No. 11347104, and the Fundamental Research Funds for the Central Universities.

Author Contributions

H.Z. conceived the concept of using the circular wave trains induced by CPEF to suppress the spiral turbulence. X.F., X.G. and J.-M.T. developed this approach and performed numerical simulations and data analysis. X.G., X. F., J.-T.P. and H.Z. contributed to the discussion about the characteristics of the induced the circular wave trains and the mechanism of suppressing the spiral turbulence. X.F., X.G., J.-T.P. and H.Z. wrote the manuscript with input from all authors.

Additional Information

Competing financial interests: The authors declare no competing financial interests.

How to cite this article: Feng, X. *et al.* Wave trains induced by circularly polarized electric fields in cardiac tissues. *Sci. Rep.* **5**, 13349; doi: 10.1038/srep13349 (2015).



This work is licensed under a Creative Commons Attribution 4.0 International License. The images or other third party material in this article are included in the article's Creative Commons license, unless indicated otherwise in the credit line; if the material is not included under the Creative Commons license, users will need to obtain permission from the license holder to reproduce the material. To view a copy of this license, visit <http://creativecommons.org/licenses/by/4.0/>